eLIFE elifesciences.org

RESEARCH ARTICLE

Figures and figure supplements

Intraneural stimulation elicits discrimination of textural features by artificial fingertip in intact and amputee humans

Calogero Maria Oddo *et al*

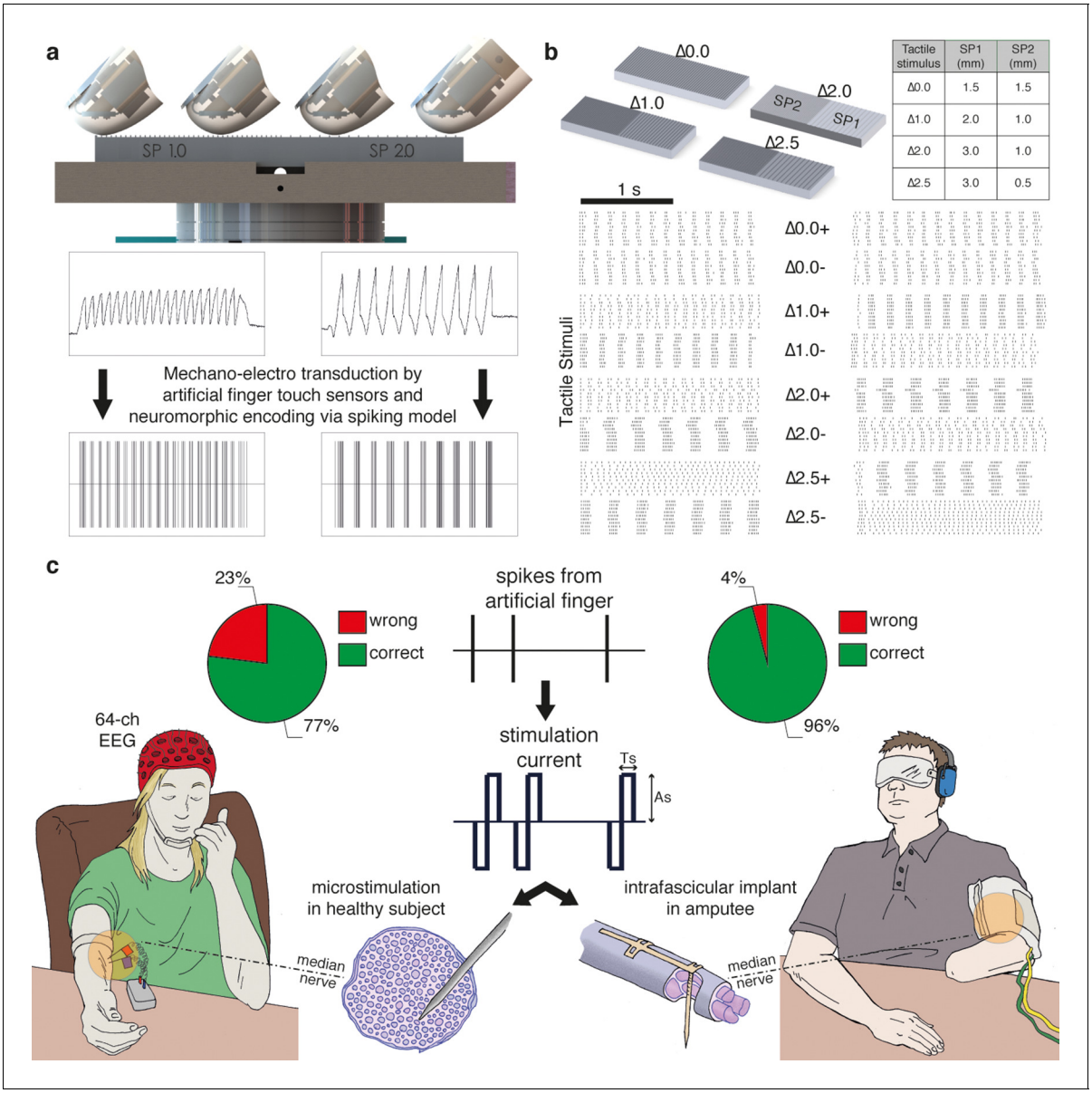

Figure 1. Experimental setup and performance metrics. (**a**) Sensorized artificial finger and tactile stimulation platform. (**b**) Tactile stimuli that were used in the three-alternative forced-choice (3AFC) psychophysical protocol and the raster plot of spike trains that were generated in all sessions with one subject by the artificial finger while the gratings were slid. (**c**) Setup of percutaneous electrical microstimulation (left) and implanted intrafascicular stimulation (right) of the median nerve, and discrimination performance during all experimental sessions involving four intact subjects and one transradial upper limb amputee.Source data of the spike trains that were transduced by the artificial finger while the gratings were indented and slid over have been deposited in Dryad (***Oddo et al., 2016***). Such spikes were used to trigger the neural stimulator in all the experimental sessions with DAS amputee (raster plot depicted in ***Figure 1b***).

DOI: 10.7554/eLife.09148.003

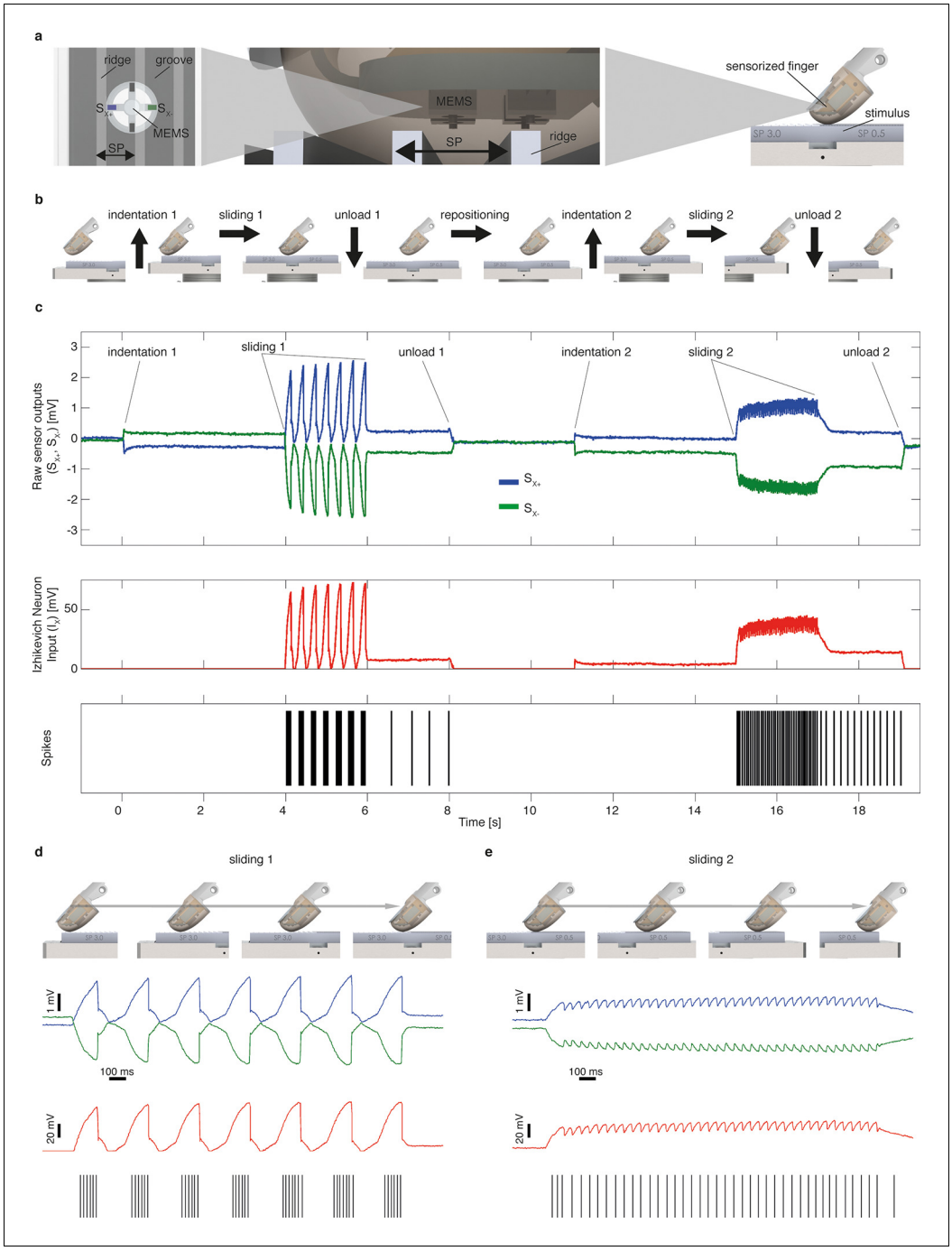

Figure 2. Mechano-neuro-transduction process. (**a**) MEMS sensor with 4 transducing piezoresistors implanted at the base of a cross-shaped structure (sensor piezoresistive outputs S_{x+} and S_{x-} are represented in blue and in green, respectively), grating with ridges and grooves that alternate with spatial period SP, and sensorized fingertip, which is in contact with tactile stimulus. (**b**) The sequence of presentation of surface pair to the artificial finger. (**c**) Example of implementation of the Izhikevich model for real-time conversion of MEMS sensor data into a sequence of artificial neural spikes. The blue and green traces show raw sensor outputs from the pair of opposing channels depicted in panel a. The red trace shows the input to the Izhikevich artificial neuron, which results from the application of ***Equation 1 and 2*** (described in the Materials and methods section). The black lines depict the spikes that are generated when the membrane potential of the Izhikevich artificial neuron reaches the threshold (***Equation 5*** in the Materials and methods section) and, thus, the neural stimulator is triggered. (**d–e**)

Figure 2 continued on next page

Figure 2 continued

Implementation of the Izhikevich model with a close-up view during the sliding motion over the first and second halves of the grating. The traces and color-coding are shown in panel c.

DOI: 10.7554/eLife.09148.004

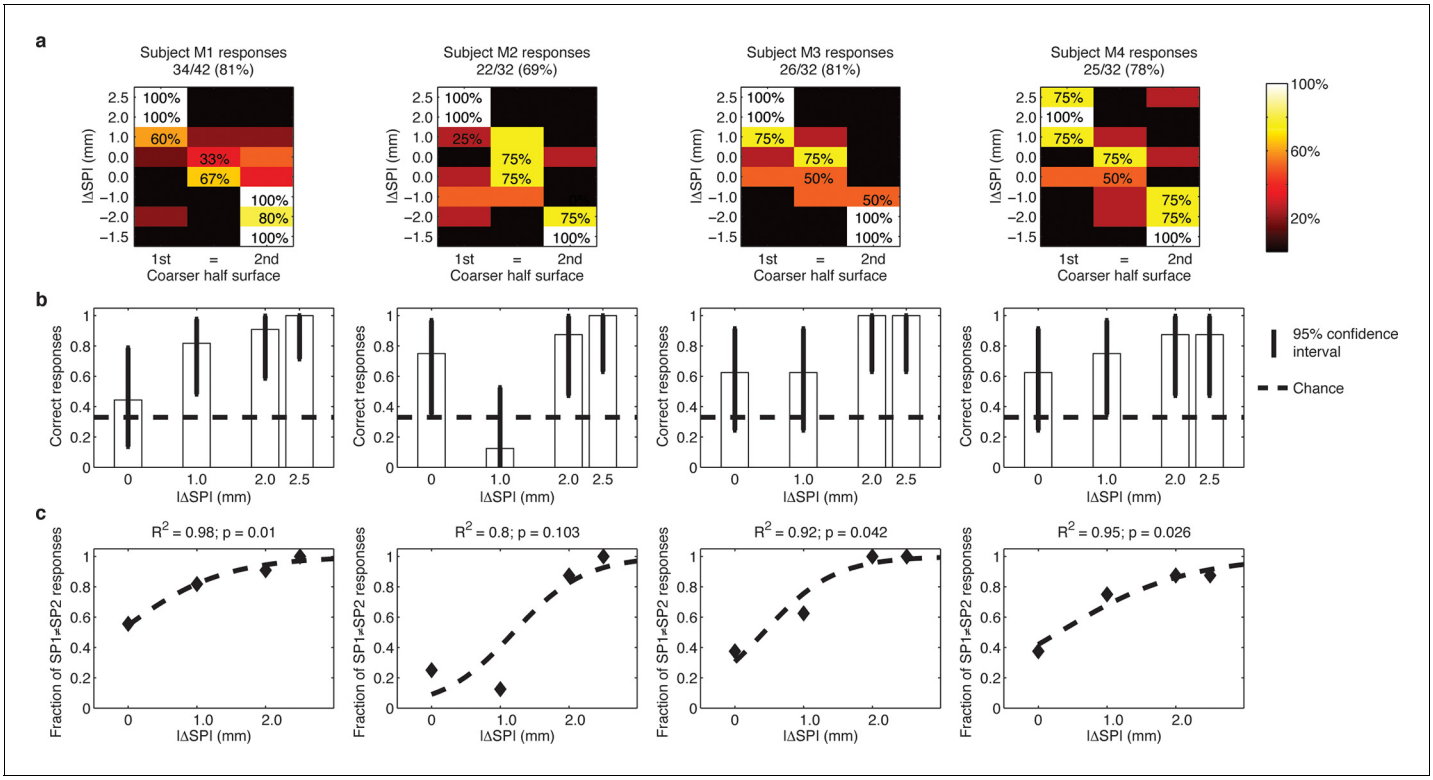

Figure 3. Responses of intact subjects during the 3AFC psychophysical protocol with percutaneous electrical microstimulation of the median nerve. Each column reports results of the analyses on individual subject basis. (**a**) Each panel displays the confusion matrix of behavioral responses relative to the four intact subjects with microstimulation. The titles indicate correct/total responses (percentage). (**b**) Vertical bars display correct responses that are associated with each stimulus. The vertical solid lines over each bar indicate the 95% confidence intervals (Clopper Pearson exact interval) per stimulus. The dashed horizontal line indicates chance level (1/3). (**c**) The fraction of trials a pair of stimuli is perceived as different as a function of difference in spatial period (ΔSP) between the two stimulus halves, and logistic fit (dashed line). The title reports the R^2 associated with the fit, i.e., the fraction of data variance explained by the logistic function, and the significance of the Pearson correlation between data points and the fit.

DOI: 10.7554/eLife.09148.005

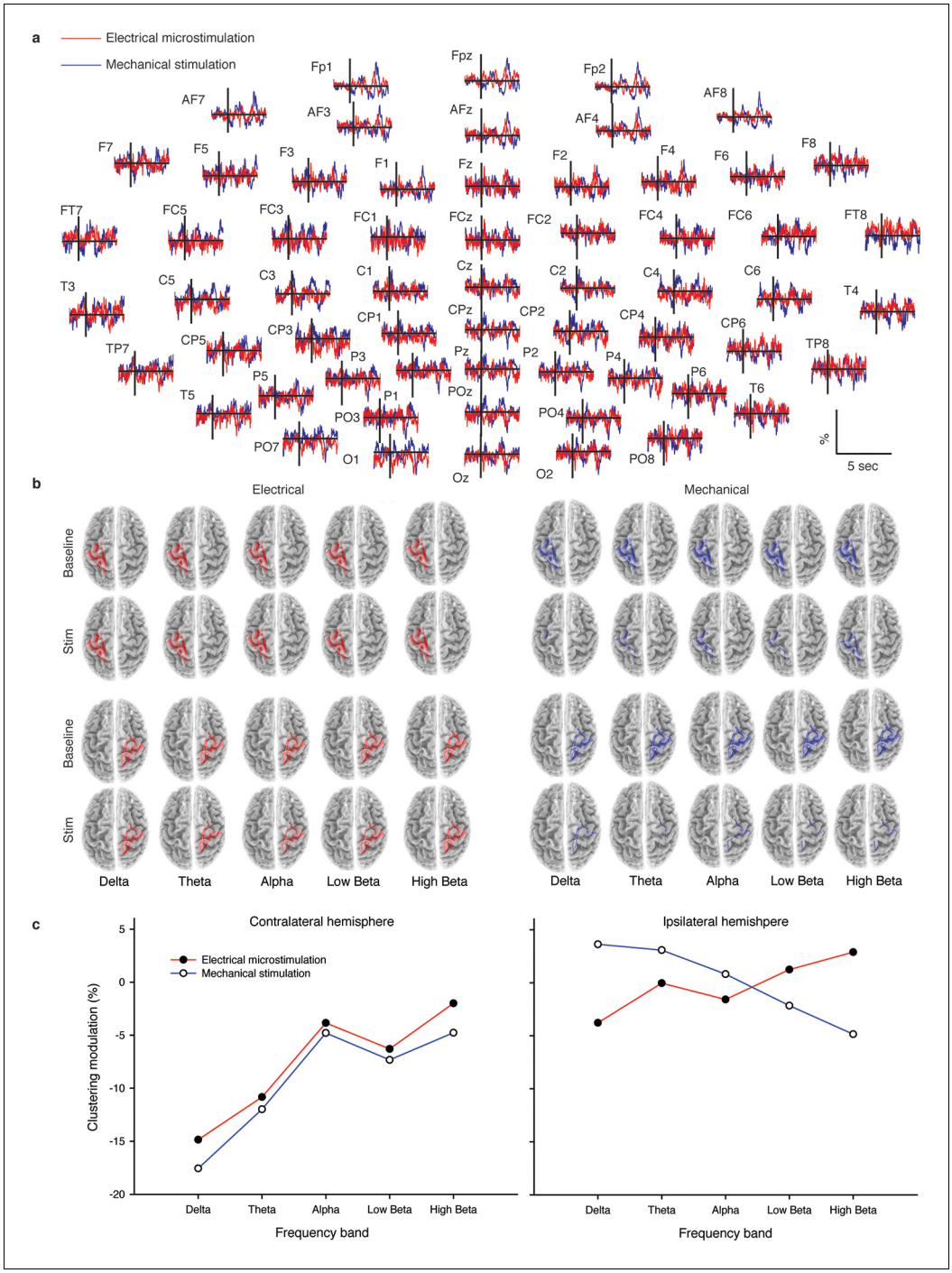

Figure 4. Cortical response to mechanical and electrical stimulation using a surface with 1.5 mm SP. (**a**) Grand average event related potentials (ERPs) of all subjects (n = 4) for both substitutive neuromorphic electrical (red) and natural mechanical tactile (blue) stimulation, ranging from -1500 to 3000 ms with respect to the stimulus onset. Each channel was normalized for the standard deviation of the prestimulus. (**b**) eLORETA connectivity maps for delta, theta, alpha, low beta and high beta bands. Each tract (red for electrical and blue for mechanical stimulations) among the 7 sensorimotor regions of interest (Brodmann Areas BA 1–7) reports the connectivity value higher than the cut-off threshold (functional coupling >0.3). (**c**) Clustering modulation (percentage of variation during stimulation with respect to baseline) in the left and right hemispheres with electrical and mechanical stimulations. A significant reduction in clustering modulation across all frequencies occurred in the hemisphere contralateral to the stimulation ($p<0.05$, comparison to the right hemisphere, Duncan test after ANOVA).
DOI: 10.7554/eLife.09148.007

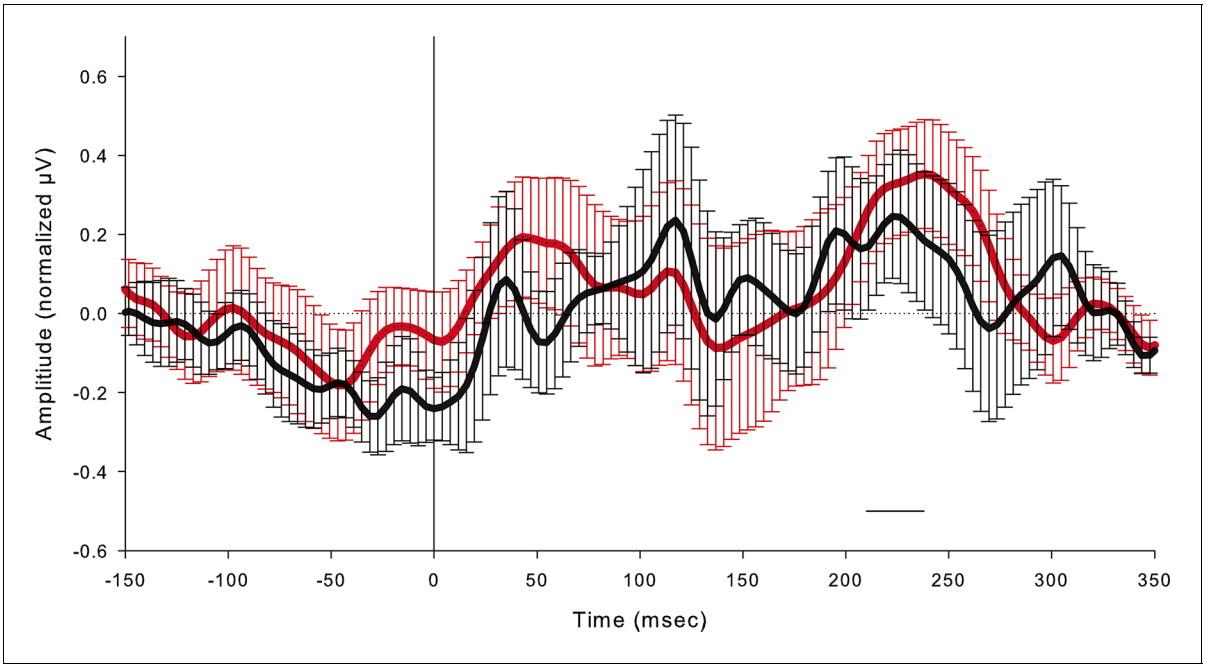

Figure 4—figure supplement 1. Grand average event related potentials (ERPs) of all subjects (n = 4) at the FC1 electrode for both the substitutive neuromorphic electrical (red) and natural mechanical tactile (black) stimulation, in the -150 to 350 ms window with respect to stimulus onset, with confidence interval bars. The horizontal black bar indicates the time window (210–240 ms) when the evoked potential reached significance compared with the prestimulus voltage (2 Standard Deviations from the mean prestimulus voltage), both after the electrical microstimulation and after the mechanical stimulation.

DOI: 10.7554/eLife.09148.008

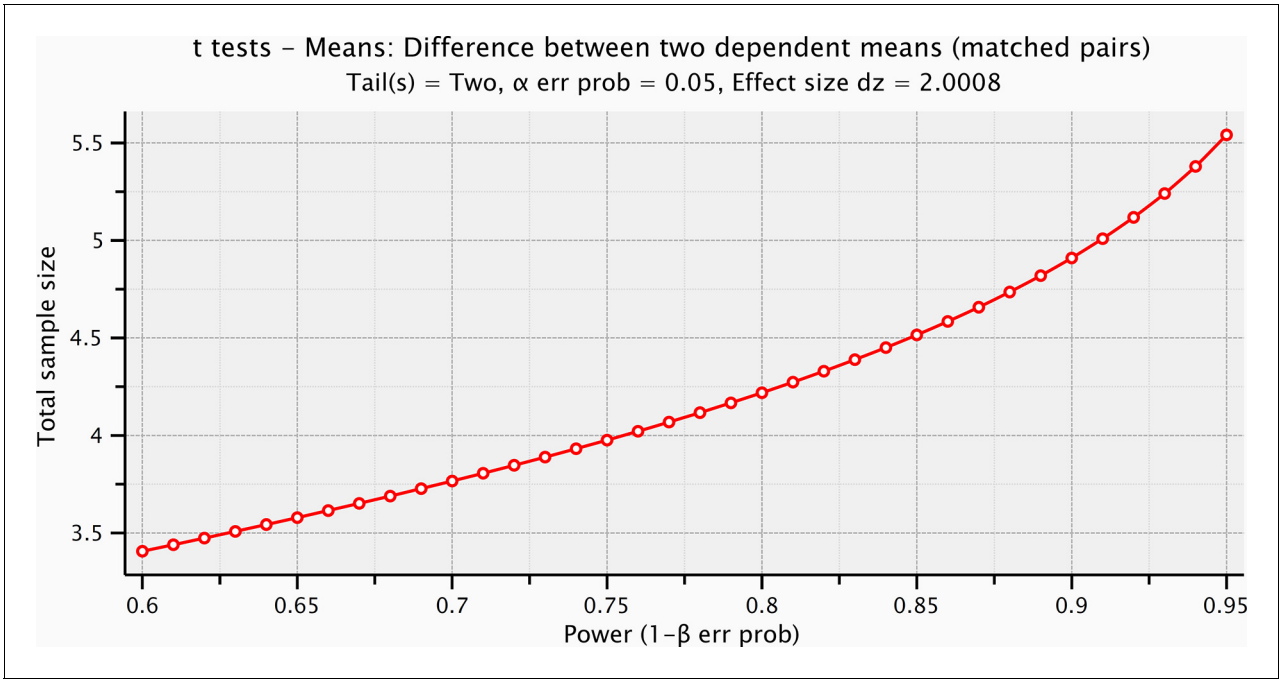

Figure 4—figure supplement 2. Sample size computation based on the effect size of the prestimulus and the evoked activity within the significant time-window for the electrical microstimulation.

DOI: 10.7554/eLife.09148.009

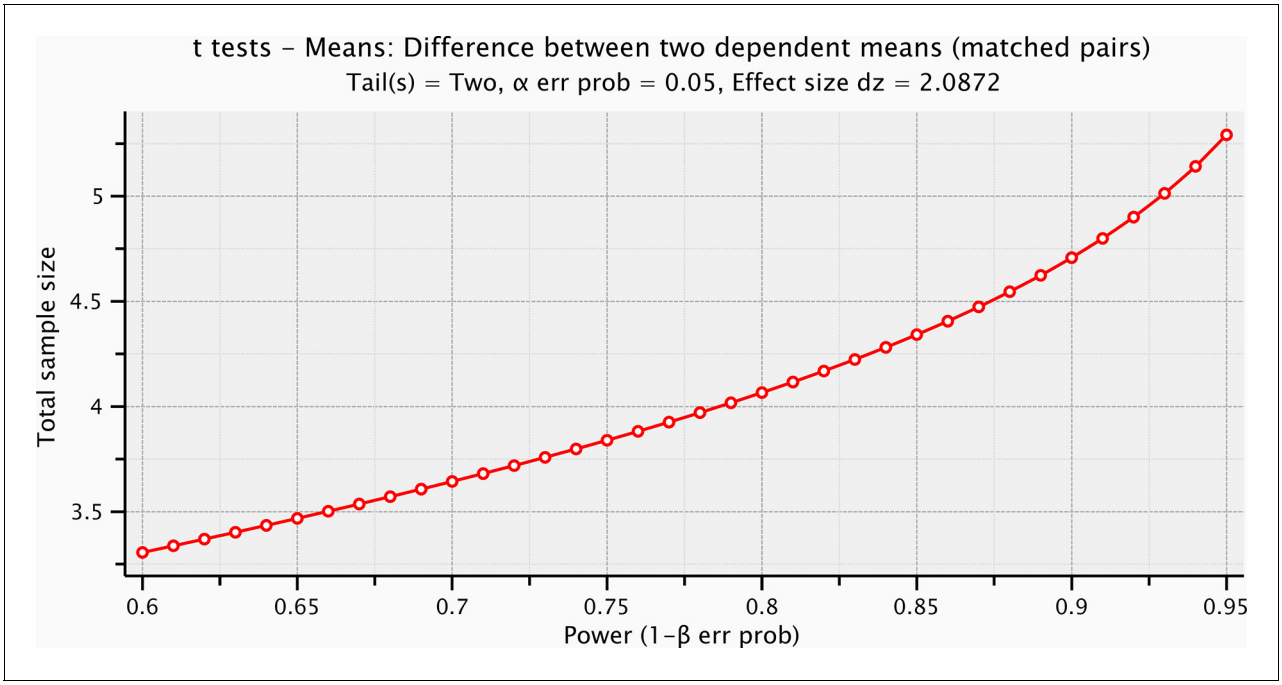

Figure 4—figure supplement 3. Sample size computation based on the effect size of the prestimulus and the evoked activity within the significant time-window for the mechanical stimulation.
DOI: 10.7554/eLife.09148.010

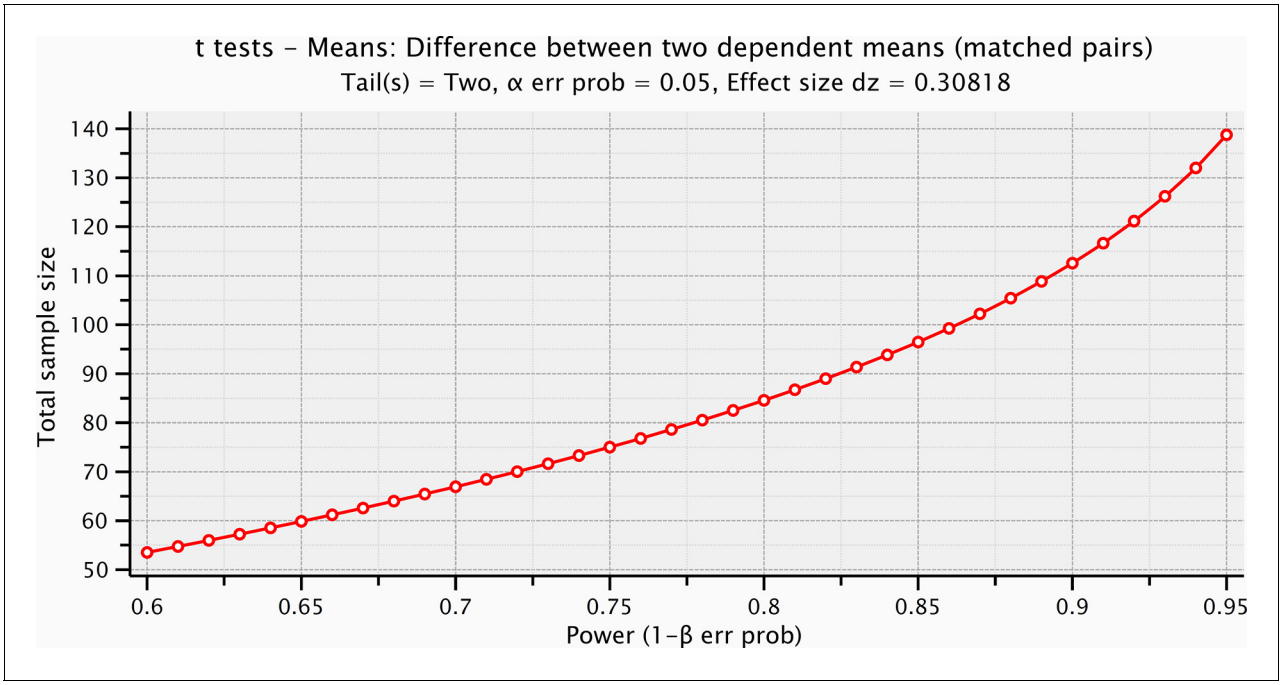

Figure 4—figure supplement 4. Sample size computation based on the prestimulus effect sizes preceding the electrical microstimulation and the mechanical stimulation.

DOI: 10.7554/eLife.09148.011

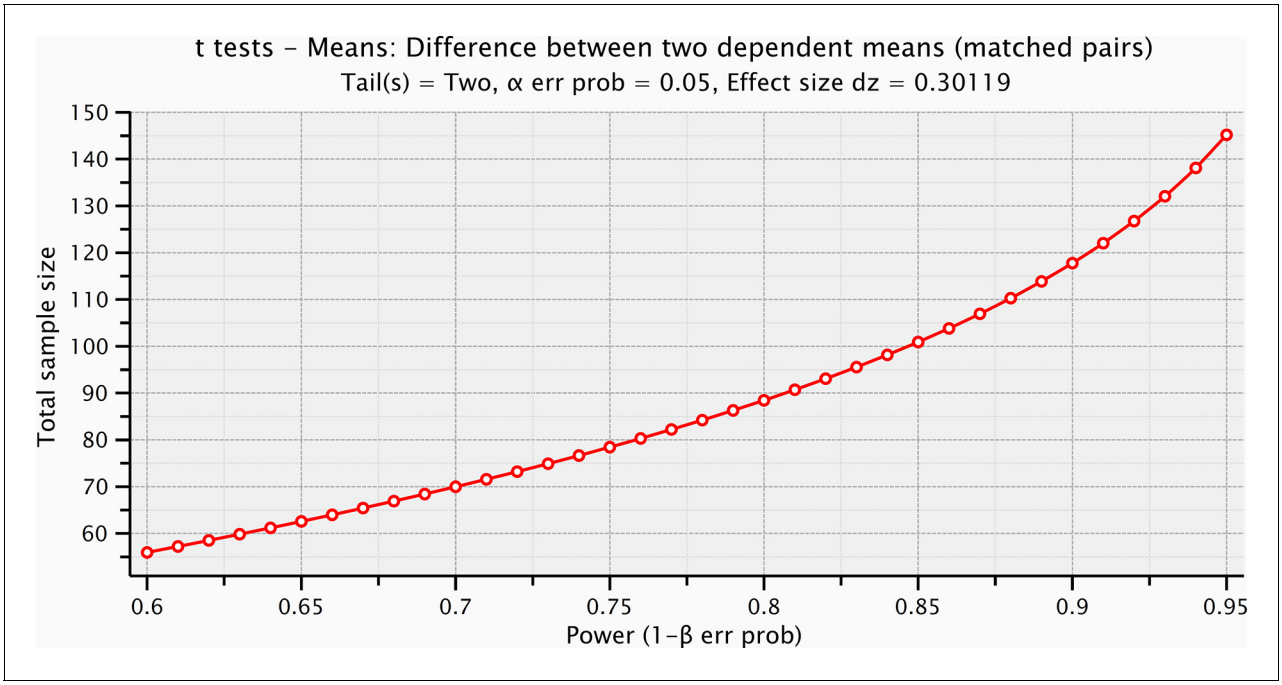

Figure 4—figure supplement 5. Sample size computation based on the effect size of the stimulus voltages (ERPs within the significant time-window after the electrical microstimulation, and after the mechanical stimulation).
DOI: 10.7554/eLife.09148.012

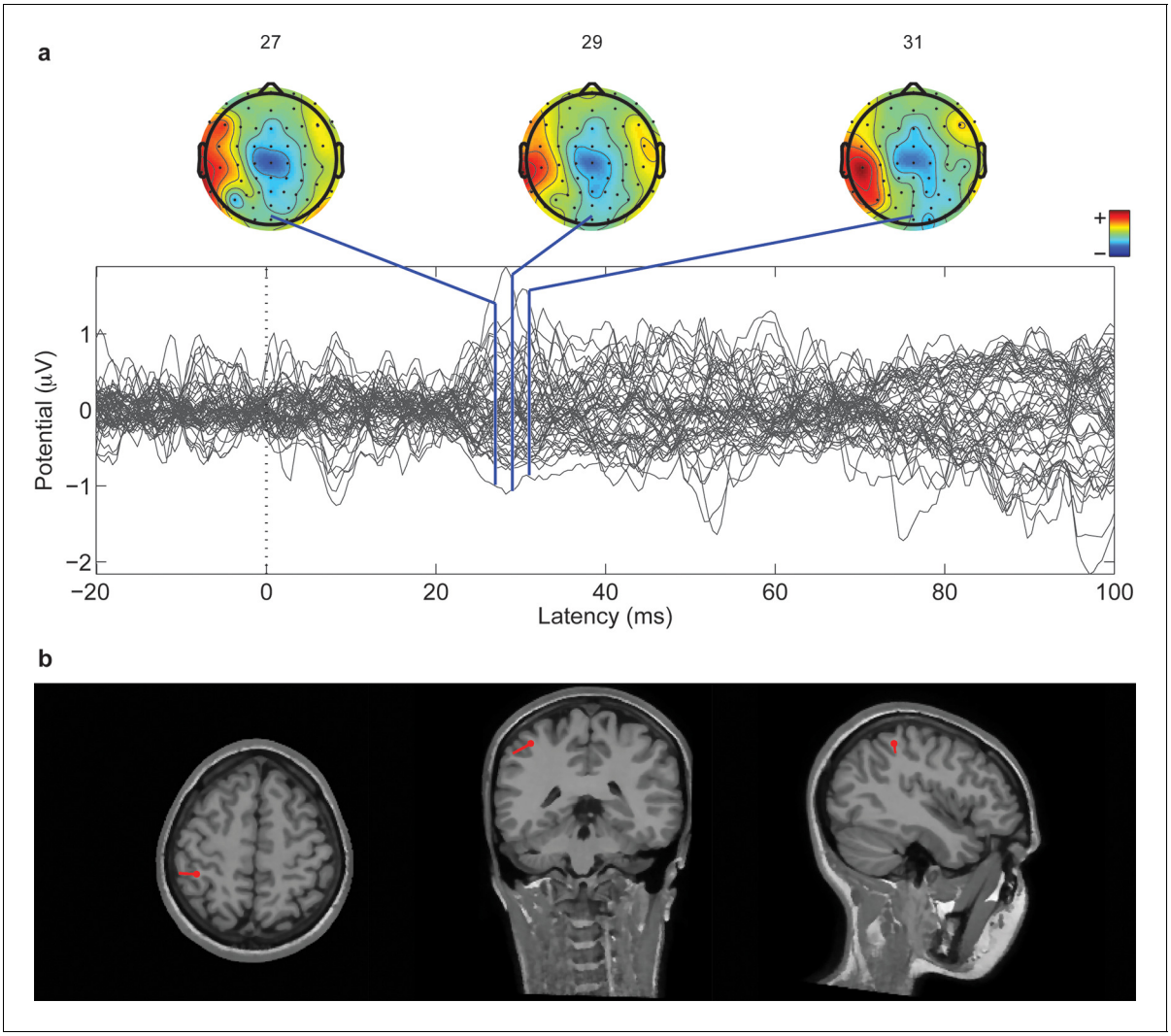

Figure 5. Cortical localization of a 1 Hz electrical microstimulation sensory evoked potential. (**a**) Butterfly plot of SEPs for all 64 channels of one subject (M4). All traces are aligned to the electrical stimulus delivery. On top, the topographic representation of amplitude distribution at different time lags (ms). (**b**) Position of the associated equivalent dipole, which corresponds to P27 peak, superimposed on the individual horizontal, coronal and sagittal structural MRI planes of the subject.

DOI: 10.7554/eLife.09148.013

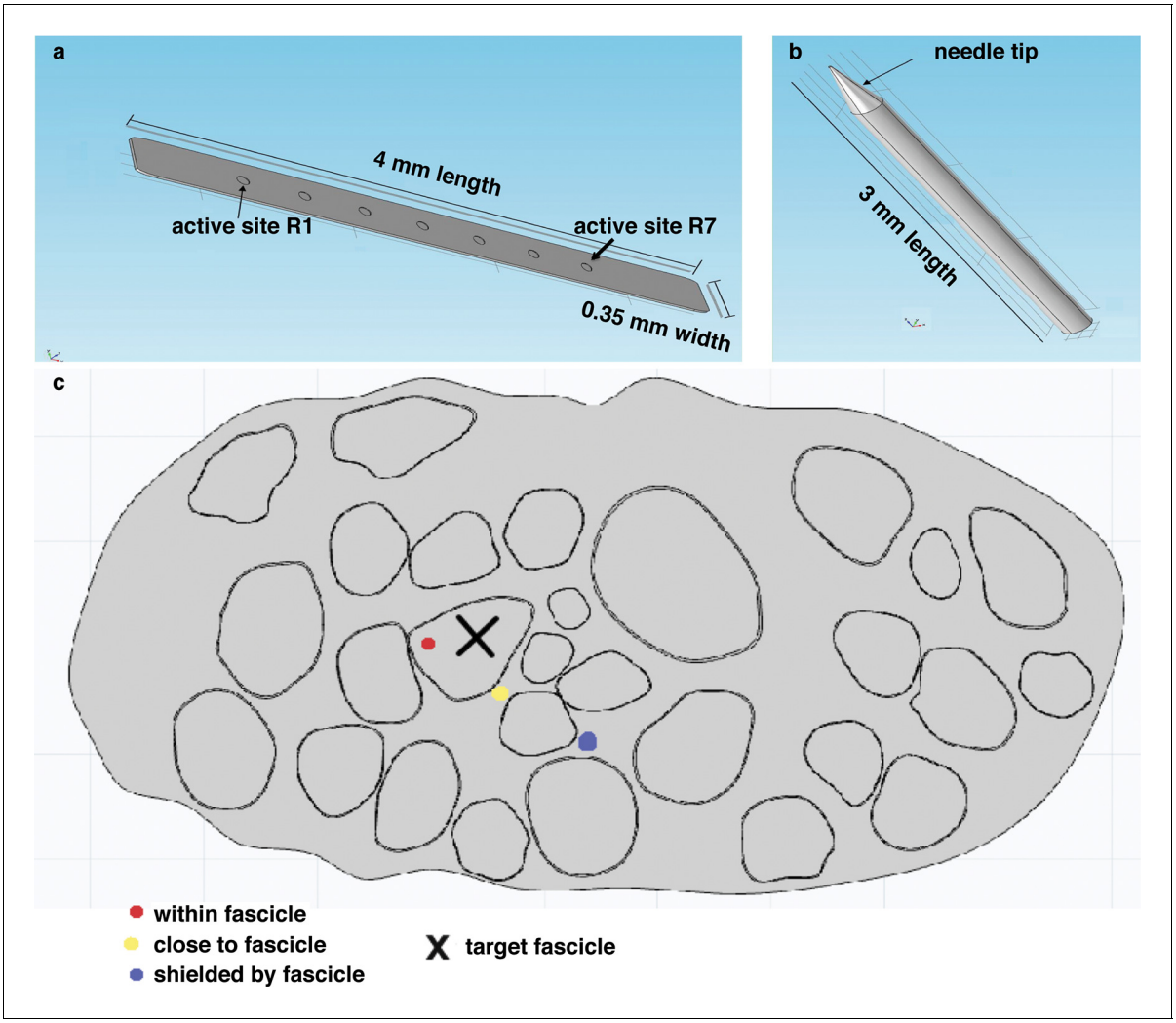

Figure 6. Representation of the physical design of electrodes for the hybrid model. (**a**) Implementation for the TIME electrode. (**b**) Implementation for the microneedle. (**c**) Different locations for stimulating active site and tip, that were used in the model to compare the TIME interface versus the microstimulation needle. Red dot represents the evaluated intrafascicular positioning of the TIME active site and the end of microstimulation needle tip. Yellow dot represents close-to-fascicle location, where the end of microstimulation needle tip and the active site of TIME interface were placed. Blue dot represents an example position with a shielding fascicle. The X marker represents the targeted fascicle, where the fiber activation was calculated for different locations of microneedle and TIME for 9 different populations that emulated biologically inherent uncertainty in the placement and extension of fibers innervating a specific hand district. This procedure was performed analogously for medium and small fascicles and confirmed the results.

DOI: 10.7554/eLife.09148.014

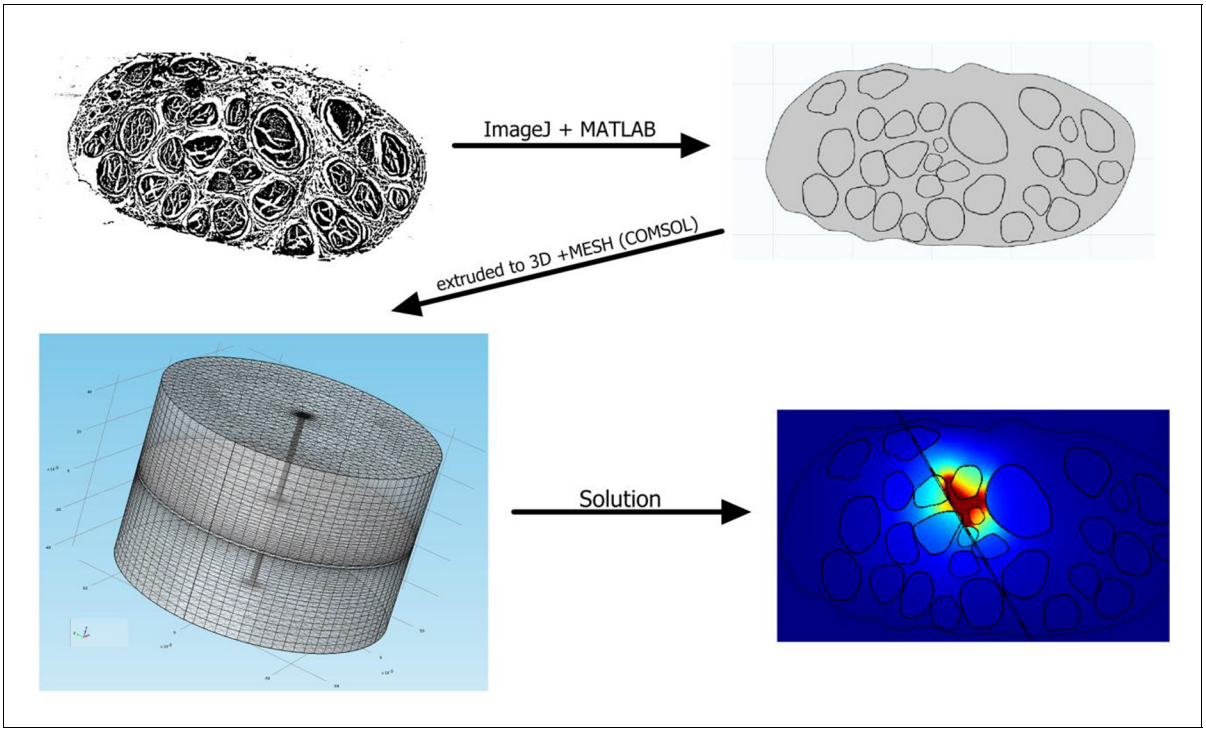

Figure 6—figure supplement 1. Finite element model development for the human median nerve, starting from histological pictures and resulting in the solution of voltage distribution within the nerve.
DOI: 10.7554/eLife.09148.015

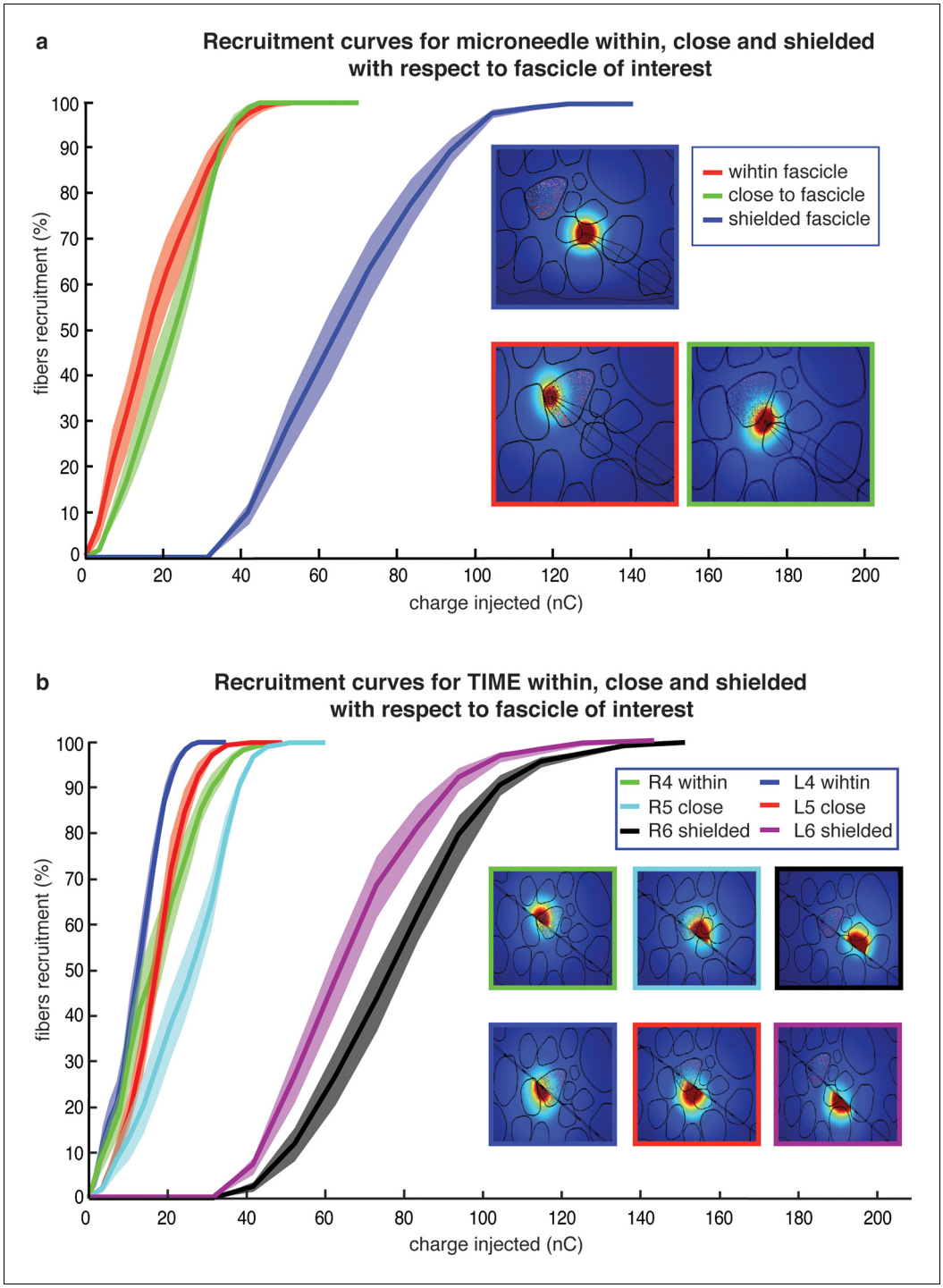

Figure 7. Comparison of needle microstimulation and TIME stimulation using hybrid FEM/Neuron models. (**a**,**b**), Recruitment curves of sensory axon populations resulting from different positions of the active sites for the needle microstimulation and TIME stimulation (mean +/- S.E.M. of percentage of recruited fibers). R4/L4 is the pair of active sites within the target fascicle; R5/L5 is close to it, and R6/L6 is shielded with respect to it. For each position of the stimulating tip/active site, nine different axonal populations were computed. The fiber was considered active when the spike travelled until the last node of Ranvier that was implemented. Figure insets represent voltage distributions for different positions of active sites, as calculated using the FEM solver. These results are representative for several electrode insertion configurations. The same computations were performed for medium and small fascicles and confirmed the results.

DOI: 10.7554/eLife.09148.016

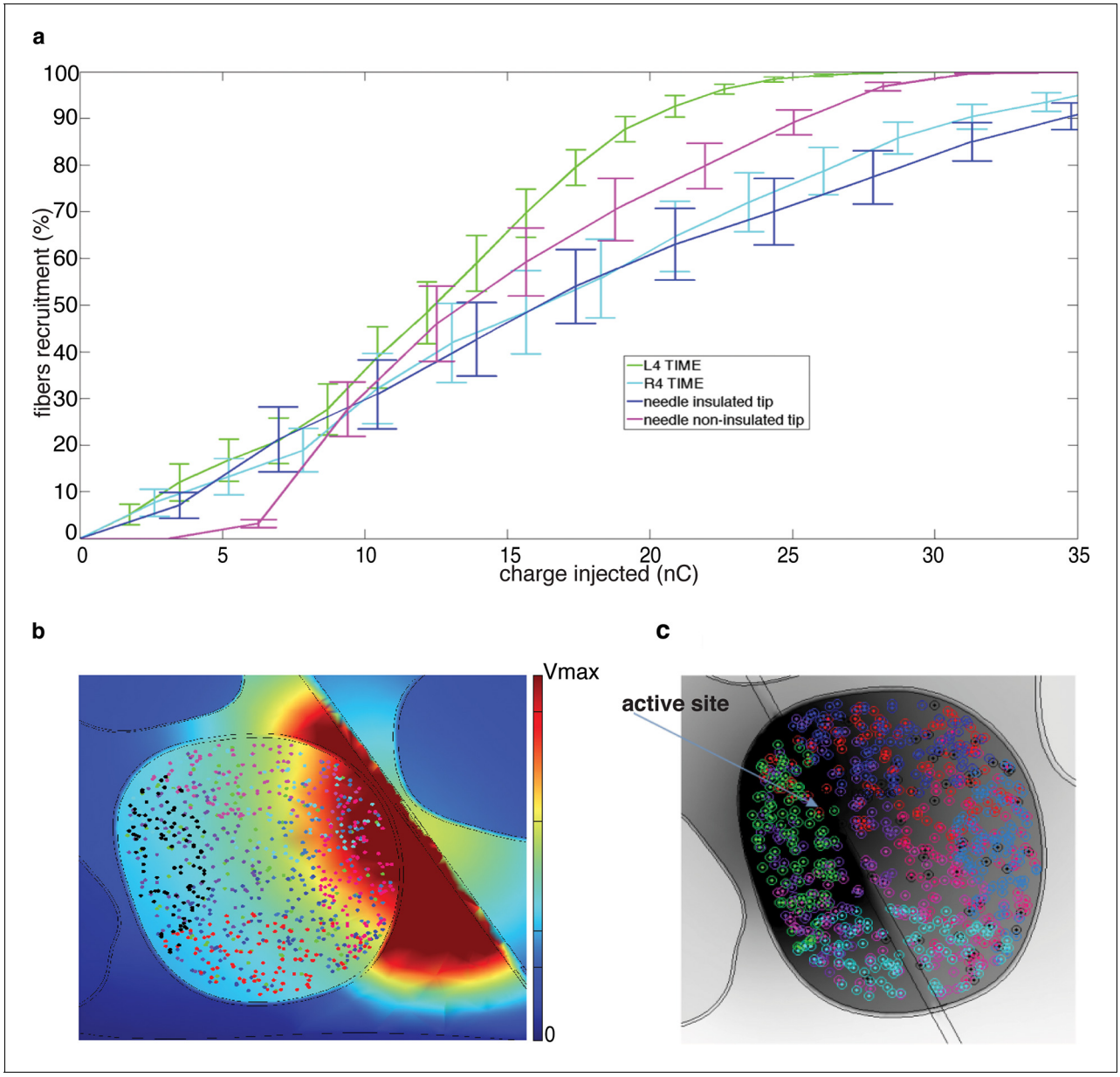

Figure 8. Fiber recruitment as a function of injected charge with microstimulation and the TIME implant. (**a**) Recruitment results obtained for placement of the microneedle tip (insulated and non-insulated tip) and the TIME active site (L4 and R4) within the fascicle of interest. The recruitment curves are the mean +/- S.E.M. for the 9 implemented populations in 4 different FEM configurations. The results for the microstimulation needle and TIME interface are similar, which supports the translation from percutaneous towards intraneural stimulation. The 2 cases of microneedle tip exposure yielded comparable outcomes. (**b**) Voltage distribution induced by the close active site and positioning of 9 different fiber populations that were implemented to emulate the inherent anatomical uncertainty of sensory axon locations (see ***Figure 8—figure supplement 1*** for the correspondence between each color of the fibers illustrated in the panel and the specific implemented population). (**c**) The colored dots indicate another randomized positioning of 9 different fiber populations implemented in the simulations of the hybrid electrical-biophysical model of the median nerve, with active site inside of fascicle.

DOI: 10.7554/eLife.09148.017

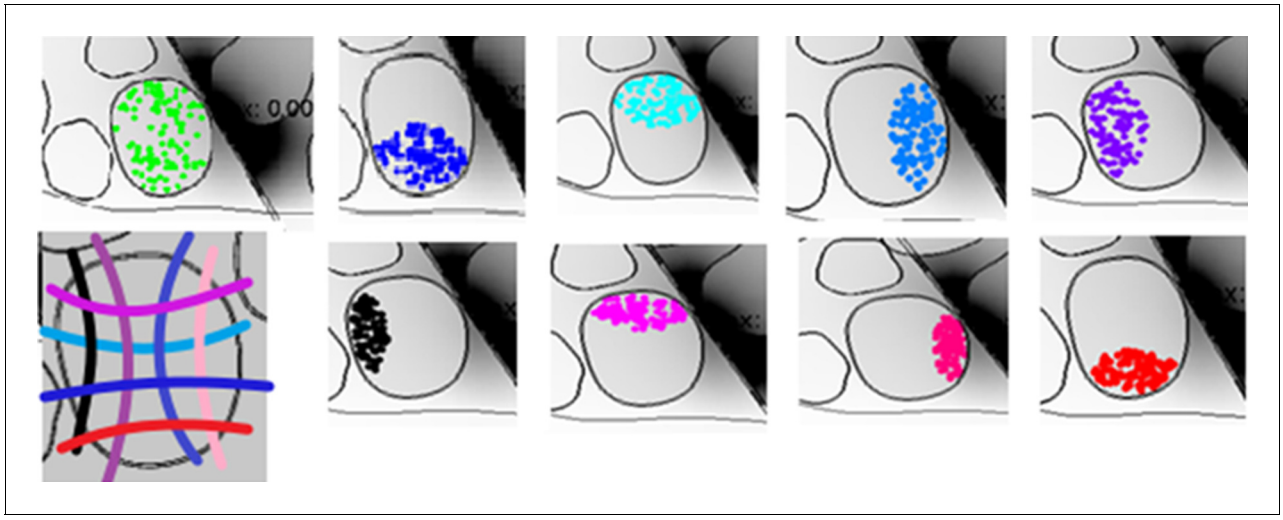

Figure 8—figure supplement 1. Representation of the 9 neural populations within large fascicles that were implemented in the hybrid electrical-biophysical model simulations to compare needle microstimulation and stimulation via implanted TIME interface.
DOI: 10.7554/eLife.09148.018

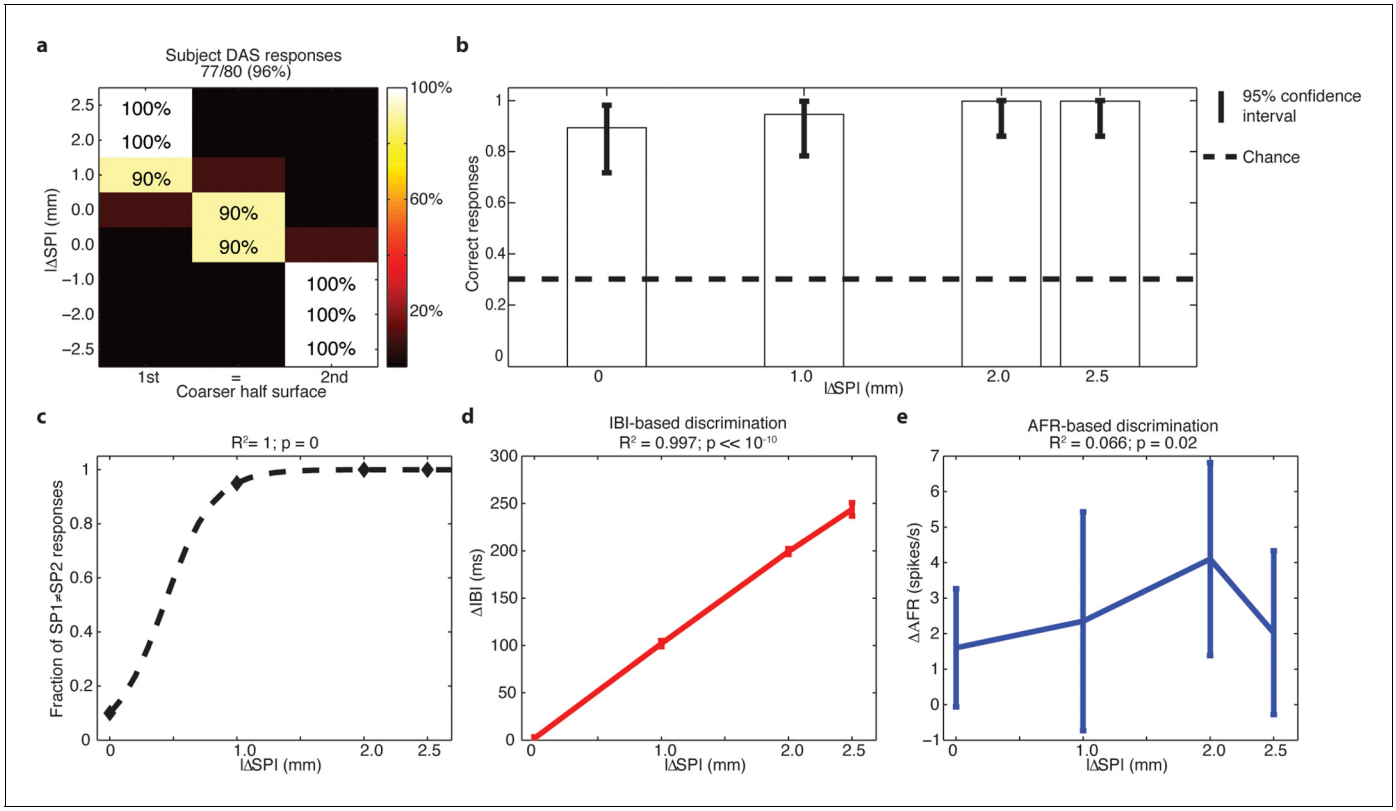

Figure 9. Subject behavior and analysis based on the stimulus spatial period (SP), inter-burst interval (IBI) and average firing rate (AFR) in the session with DAS amputee. (**a**) Confusion matrix of the responses given by DAS subject. (**b**) Vertical bars display the correct responses, which are associated with each stimulus. The vertical solid lines over each bar indicate the 95% confidence intervals (Clopper Pearson exact interval) per stimulus. The dashed horizontal line indicates chance level (1/3). (**c**) Fraction of trials for which a pair of stimuli is perceived as different as a function of the difference in spatial period (ΔSP) between the two stimulus halves, and logistic fit (dashed line). The title reports the R^2 associated with the fit, i.e., the fraction of data variance explained by the logistic function, and the significance of the Pearson correlation between data points and the fit. (**d,e**) Comparison between IBI-based and AFR-based discrimination. Difference between IBIs (ΔIBI, panel d) and difference between AFRs (ΔAFR, panel e) measured in the spike patterns elicited by the two sides of each stimulus and plotted as a function of the difference between grating SPs (ΔSP). Error bars indicate the interquartile range. The title reports the fraction of explained variance.

DOI: 10.7554/eLife.09148.019

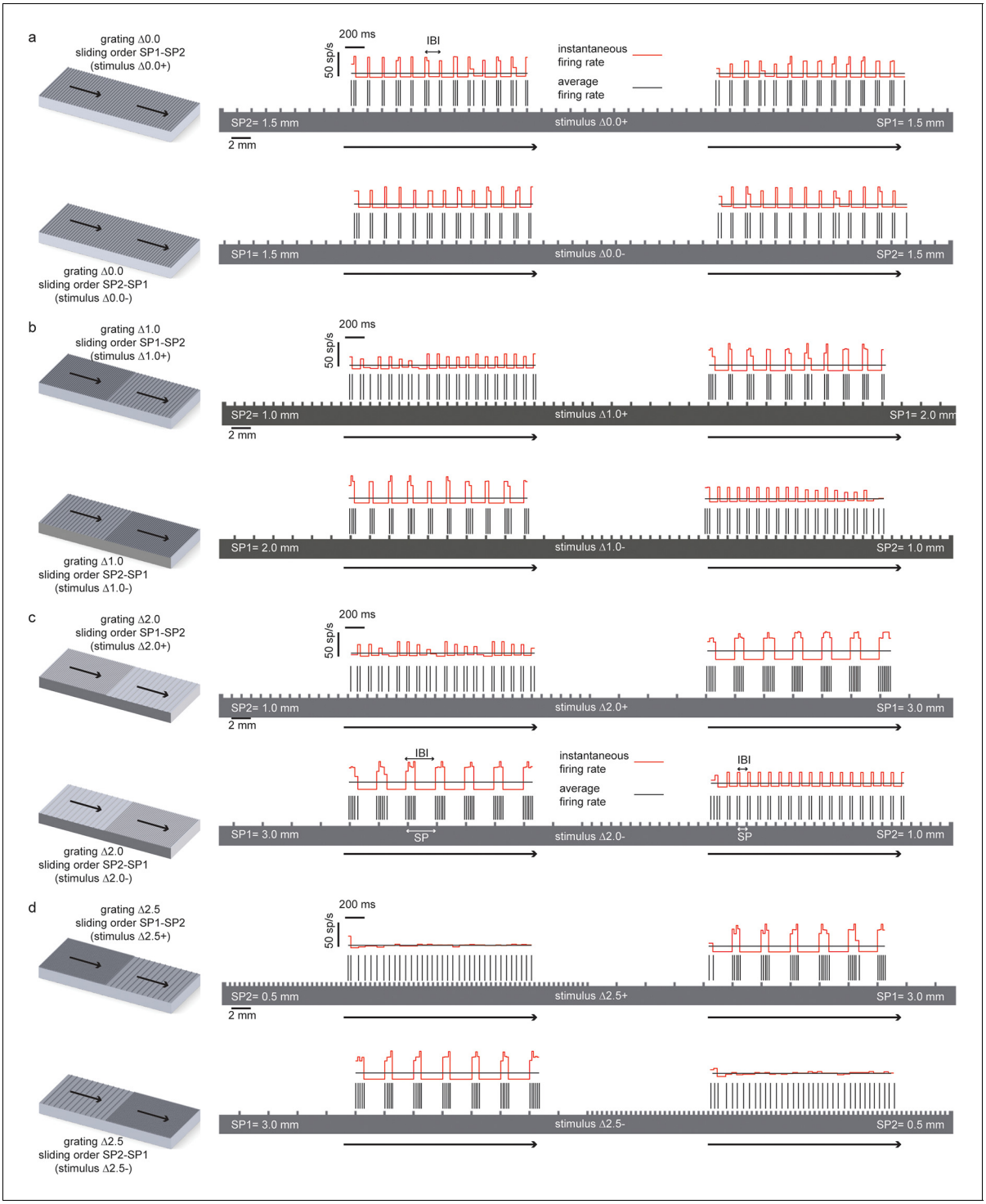

Figure 10. Temporal coding of the spatial features of the experimented tactile stimuli. In all panels the spatial structure (scale: 2 mm) of the grating is superimposed over a sample temporal pattern (scale: 200 ms) of the spike train that was obtained as a result of transduction with the artificial finger. The ratio between the spatial and temporal scales turns into the stimulus sliding velocity (10 mm/s). The instantaneous firing rate (scale: 50 spikes/s) is shown together with the average firing rate during the stimulus sliding motion. (**a**) (above) Stimulus Δ0.0+ is characterized by thw presentation of two half surfaces in the SP1 - SP2 order (first: 1.5 mm, second: 1.5 mm); (below) stimulus Δ0.0-, is characterized by the presentation of two half surfaces in the SP2 – SP1 order (first: 1.5 mm, second: 1.5 mm). For stimulus Δ0.0, the two half surfaces have the same coarseness. Therefore, Δ0.0+ and Δ0.0- result in spiking patterns with a common temporal structure. (**b**), (above) Stimulus Δ1.0+ is characterized by the presentation of two half surfaces in the SP1 - SP2 order (first: 2.0 mm, second: 1.0 mm); (below) stimulus Δ1.0- is characterized by the presentation of two half surfaces in the SP2 – SP1 order

Figure 10 continued on next page

Figure 10 continued

(first: 1.0 mm, second: 2.0 mm). (**c**) (above) Stimulus Δ2.0+ is characterized by the presentation of two half surfaces in the SP1 - SP2 order (first: 3.0 mm, second: 1.0 mm); (below) stimulus Δ2.0- is characterized by the presentation of two half surfaces in the SP2 – SP1 order (first: 1.0 mm, second: 3.0 mm). (**d**) (above) Stimulus Δ2.5+ is characterized by the presentation of two half surfaces in the SP1 - SP2 order (first: 3.0 mm, second: 0.5 mm); (below) stimulus Δ2.5- is characterized by the presentation of two half surfaces in the SP2 – SP1 order (first: 0.5 mm, second: 3.0 mm).
DOI: 10.7554/eLife.09148.020

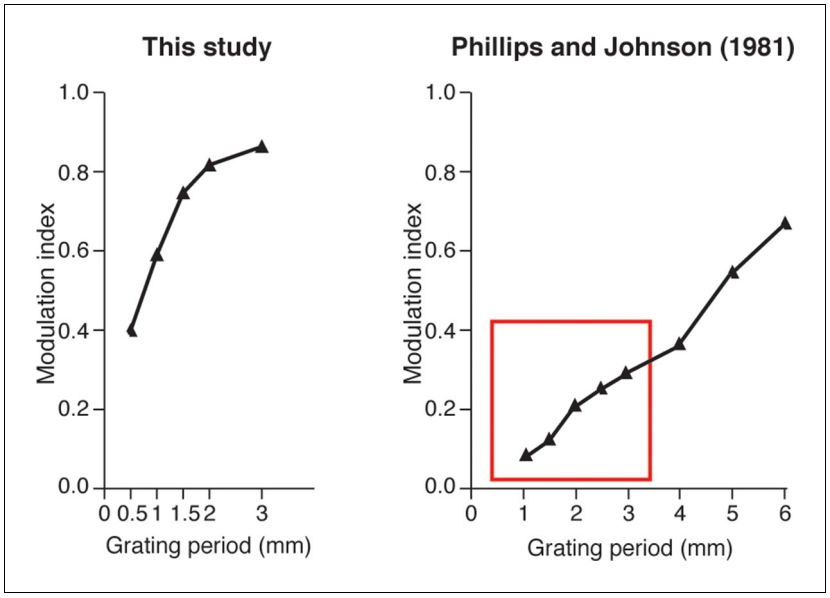

Figure 10—figure supplement 1. Spatial modulation index that was calculated from the artificial-touch spike patterns from our study (left) compared to neurophysiological data shown by Phillips and Johnson for SA1 units (right, adapted from a previous study (***Phillips and Johnson, 1981***). The depicted spatial modulations have the same monotonic trend versus the period of grating. The spatial modulation of our spike trains is globally higher in comparison with the neurophysiological data that was previously shown (***Phillips and Johnson, 1981***) for surfaces with the same spatial period (highlighted by a red box in the figure). We hypothesize that this difference exists because our surfaces had a constant ridge width of 0.25 mm, whereas, the surfaces in the study performed by Phillips and Johnson were square-wave gratings (i.e., ridge width was equal to groove width and was equal to half the spatial period).

DOI: 10.7554/eLife.09148.021